Thin Solid Films 687 (2019) 137462

Contents lists available at ScienceDirect

Thin Solid Films

journal homepage: www.elsevier.com/locate/tsf

Synthesis and characterization of styrene-based polyfluoroacrylate film for hydrophobic/icephobic applications

Tamal Barman[a], Hao Chen[b], Junpeng Liu[a], Guang Yang[c], Wenjie Zhao[d], Chuang Peng[b], Xianghui Hou[a,*]

[a] Faculty of Engineering, University of Nottingham, University Park, Nottingham NG7 2RD, UK
[b] Faculty of Science and Engineering, University of Nottingham Ningbo China, Ningbo 315100, China
[c] Key Laboratory of Aerospace Materials and Performance, Ministry of Education, School of Materials Science and Engineering, Beihang University, Beijing 100191, China
[d] Key Laboratory of Marine Materials and Related Technologies, Zhejiang Key Laboratory of Marine Materials and Protective Technologies, Ningbo Institute of Materials Technology and Engineering, Chinese Academy of Sciences, Ningbo 315201, China

ARTICLE INFO

Keywords:
Polyfluoroacrylate
Polymerization
Hydrophobicity
Icephobicity

ABSTRACT

Low surface energy polymeric materials always attract great interest due to their effective non-stick feature when contacting with other materials. In the present work, hydrophobic polyfluoroacrylates (PFAs) were synthesized using styrene, acrylic acid, and heptafluorobutyl acrylate via radical polymerization. The synthesized PFA emulsions had a relatively low curing temperature (e.g. 80 °C), and different molar ratios of heptafluorobutyl acrylate were used to vary the fluorine content in the PFAs. From chemical analysis by Fourier transform infrared spectroscopy, X-ray photoelectron spectroscopy, and nuclear magnetic resonance, it was found that the synthesized PFA emulsion exhibited *co*-polymer structure consisting of the three monomer units. PFA films were deposited on aluminium substrates by spin coating of the synthesized emulsions. The hydrophobicity of the films varied with the fluorine content, and a maximum water contact angle of 121° was achieved under relatively smooth surface condition. Ice adhesion of the PFA films was also evaluated using a centrifugal method, and the ice adhesion strength decreased with the increase of the fluorine content in PFA.

1. Introduction

Hydrophobic and superhydrophobic surfaces have received increasing attention in aerospace, automotive and oil & gas industries due to the unique potentials for anti-corrosion and self-cleaning applications [1–4]. Atmospheric icing often causes severe and fatal hazards in power lines, telecommunications, wind turbine blades, as well as on the surface of aircraft [5]. The origin of the hydrophobicity/superhydrophobicity mainly comes from the natural lotus leaves where the incident water droplet rolls off the surface rapidly without wetting the surface [6]. It is generally recognised that the modification of surface profiles and the deposition of coating materials are effective in achieving hydrophobic or even superhydrophobic surfaces [7,8]. Many processes have been used to create the required rough surface, i.e. chemical etching [9], anodising [10], and sol-gel [11], etc. Work concerned on this aspect has been widely reported and microscale or nanoscale surface roughness can be obtained if the process parameters are carefully controlled [12–14]. In addition to surface modification, low surface energy is the key controlling factor in the fabrication of superhydrophobic surfaces. Low surface energy coating has also been proposed for providing icephobic surfaces. Such coatings appear to be effective in minimising the water/ice accumulation at the surface. For examples, polycarbonate coated superhydrophobic surface led to a significant decrease in ice-adhesion strength for aluminium samples as compared to the untreated reference [15]. A sol-gel coating of methyl triethoxysilane (MTEOS) and 3 –glycidyloxypropyl triethoxy silane (GLYMO) was reported to obtain a robust icephobic coating with water contact angle (WCA) as high as 163.5° and ice adhesion strength is lowered by 40% [16]. Self-assembling monolayers produced by varying hydrophobic components had also been used for icephobic application [17]. Among the available low surface energy coatings, polymeric materials are the most promising candidates as they are inherently hydrophobic [18–20]. It was reported that the water contact angle on a micro-structured Poly(tetrafluoroethylene) (PTFE) coated surface can be as high as 164° with contact angle hysteresis (CAH) of 2.5° [21]. And a polydimethylsiloxane (PDMS) based surface exhibited a water contact angle of 160° [22]. Other types of polymer coatings had also demonstrated hydrophobic behaviour [21,23,24]. Besides, slippery liquid-

* Corresponding author.
E-mail address: xianghui.hou@nottingham.ac.uk (X. Hou).

https://doi.org/10.1016/j.tsf.2019.137462
Received 8 April 2019; Received in revised form 30 June 2019; Accepted 13 July 2019
Available online 05 August 2019
0040-6090/

infused porous surfaces were developed recently and have shown encouraging icephobic properties [25]. However, low mechanical properties of the coating materials, high processing temperature (e.g. 327 °C melting temperature of PTFE [26]) and usage of lubricating liquid on the surface are the key challenges for their applications.

Modified polymers with certain functional groups which exhibit enhanced hydrophobicity are of particular interest since their chemical and mechanical properties can be carefully tailored by varying the content of monomers [18,27,28]. Icephobicity, on the other hand, is the ability of a solid surface to reduce or prevent the ice formation and hydrophobic surfaces with low surface energy are often used for icephobic applications [29,30]. It is reported that ice adhesion strength increases and water drop freezing time decreases with the decrease in surface free energy but there is no direct relationship between ice accretion and solid wettability [31]. Reduced surface energy decreases the shear adhesion stress and hence the ice adhesion strength on the surface [16]. Ice adhesion strength correlates with water contact angle only when the surfaces have similar roughness. Ice adhesion strengths on low surface energy coated substrates with higher surface roughness may be much higher than those with a smoother surface [32]. Again, ice adhesion strength of oil infused polymer surface is much lower as compared to superhydrophobic polymer surface [33]. There is an argument on the effect of superhydrophobicity induced by high surface roughness, as the surface asperities may raise the ice interaction via mechanical interlocking [34]. Therefore, synthesizing new polymeric materials with low surface energy is believed to be a sensible long-term solution for the R&D of icephobic coatings. Ice adhesion strength corelates strongly with the work of adhesion required to remove a liquid water drop from the substrate surface, and the strength was reduced by 4.2 times when the substrate is coated with a low surface energy material [35].

The present work attempts to synthesize a polyfluoroacrylate (PFA) emulsion with low curing temperature, high hydrophobicity, and improved icephobicity. The emulsion has been synthesized by a radical initiated polymerization reaction of styrene, acrylic acid, and heptafluorobutyl acrylate. Since the fluorine content is closely related to the heptafluorobutyl acrylate, various molar ratios of heptafluorobutyl acrylate are used. The polymer is thermoset in nature and the chemical composition is characterized by Fourier transform infrared spectroscopy (FTIR), X-ray photoelectron spectroscopy (XPS), and nuclear magnetic resonance (NMR) analysis. The hydrophobicity of the PFA emulsion is quantified through WCA measurements, and ice adhesion strength of the PFA films was evaluated by a centrifugal method.

2. Experimental methods

2.1. Chemicals

Styrene (purchased from Sigma Aldrich), acrylic acid (purchased from Alfa Aesar), hydroxyl propyl acrylate (purchased from Sigma Aldrich), heptafluorobutyl acrylate (purchased from Fluorochem), sodium dodecyl sulfate (SDS, purchased from ACROS organics) and potassium persulfate (KPS, purchased from Fluorochem) were used for the PFA synthesis.

2.2. Polyfluoroacrylate emulsion synthesis

A *co*-polymer of styrene, acrylic acid, and heptafluorobutyl acrylate was synthesized where SDS and KPS were used as the emulsifier and initiator, respectively. Styrene, acrylic acid, and heptafluorobutyl acrylate were mixed at different molar ratios with constant stirring. The molar ratio of styrene and acrylic acid was kept constant to 1, and the ratio of heptafluorobutyl acrylate/styrene varied from 0.5 to 2. The prepared mixture was added to 20 mL of 31 g/L SDS aqueous solution and homogenised with a high-speed homogenizer for 15 mins. In parallel, 50 mL water was taken in a three-necked round bottomed flask in a water bath at 80 °C. The flask was connected with a reflux condenser. The mixture prepared above was added to the round bottom flask dropwise with constant stirring simultaneously with 10 mL 42 g/L KPS aqueous solution. The mixture and KPS solution were added to the flask throughout 1 h. Then the mixture was refluxed for 2 h at 80 °C, followed by cooling overnight to allow the polymerization to complete.

Two types of PFA emulsions were synthesized and named as PFA 10.1 and PFA 10.2. PFA 10.1 came from styrene, acrylic acid, and heptafluorobutyl acrylate in the molar ratio of 1:1:1; while PFA 10.2 contained the same precursors in the ratio of 1:1:2. Other experimental conditions were identical.

2.3. Preparation of PFA film

The synthesized PFA emulsions were then deposited onto aluminium 1050 plates with dimensions of 25 mm × 15 mm × 1 mm via spin coating process using a Chemstat spin coater. The spin coating operation was conducted at a rotation speed of 500 rpm for 1 min and repeated for 3 times. The coated samples were then cured in an oven in a temperature range of 80–180 °C. The cured samples were then cooled to room temperature for further characterization.

2.4. Microstructural characterization

The synthesized PFA emulsion was characterized by FTIR and NMR spectra. A Perkin Elmer Spectrum one FTIR spectrometer operating at attenuated total reflection (ATR) mode was used. Transmittance in percentage was measured against wavenumber in the range of 4000 to 500 cm^{-1}. The scan was performed and averaged for 4 times. A Bruker Advance III spectrometer operating at a 19F Larmor frequency of 564.7 MHz was used for NMR analysis. Three types of NMR processes were performed, namely ^{1}H, ^{13}C, and ^{19}F NMR. An X-ray photoelectron spectroscopy (XPS, Kratos Axis Ultra Dld, Kratos Analytical Limited) was used to conduct the chemical analysis of the PFA films using Al Kα X-ray as the radiation source and the data was processed using CasaXPS software.

2.5. Surface hydrophobicity and roughness

A First Ten Angstroms FTA200 dynamic contact angle system was used for measuring the WCA of the PFA films. The surface topography and roughness were investigated by an Optical Profiler (Zeta - 20). The average surface roughness values (Ra) of aluminium substrate, PFA 10.1, and PFA 10.2 were listed in Table 1, ranging from 0.219 to 0.228 μm. Overall, all the studied surfaces were under relatively smooth condition.

2.6. Thermal characterization

For the characterization of thermal behaviour of the PFA emulsion, differential scanning calorimetry (DSC) and thermogravimetric analysis (TGA) were carried out. SDT Q600 was used for the analysis from room temperature to 200 °C, with heating rate of 2 °C/min in air environment.

Table 1
Average surface roughness values (Ra) of aluminium substrates uncoated and coated with PFA films.

Samples	Average surface roughness (μm)
Untreated aluminium 1050	0.228 ± 0.008
Aluminium coated with PFA 10.1 film	0.219 ± 0.014
Aluminium coated with PFA 10.2 film	0.222 ± 0.006

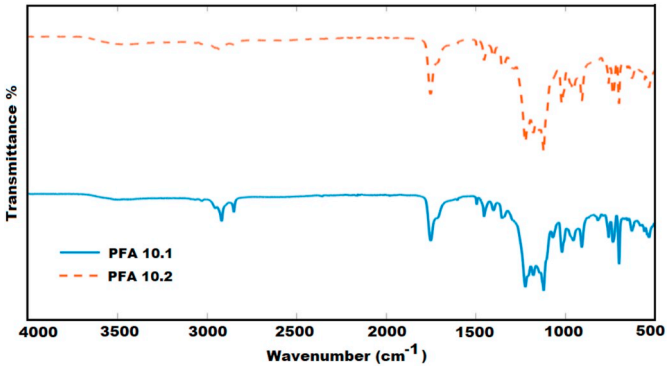

Fig. 1. FTIR spectra of PFA emulsion synthesized from 1:1:1 and 1:1:2 M ratio of styrene, acrylic acid, and heptafluorobutyl acrylate PFA10.1 and PFA 10.2 respectively.

2.7. Ice adhesion tests

Ice adhesion tests were performed by a centrifuge adhesion test method [36]. A rotor holding the ice/substrate sample on one end and the same weight on the other end was rotated at increasing rotation speed. When the centrifugal force on the ice induced by the rotation overcame the ice adhesion strength, the ice detached from the sample surface. Then the adhesion force (F) of ice on the sample surface could be estimated as $F = mr\omega^2$, where m is the mass of ice, r is the rotor length and ω is the speed of rotation at the detachment in rad/s. Then the adhesion stress τ could be calculated as $\tau = F/A$, where A is the ice/substrate contact area.

3. Results and discussion

3.1. FTIR and XPS analysis

Fig. 1 shows the FTIR analysis of a PFA emulsion synthesized from styrene, acrylic acid, and heptafluorobutyl acrylate with a molar ratio of 1:1:1 and 1:1:2. As compared to PFA 10.1, the used heptafluorobutyl acrylate is doubled for PFA 10.2. Both PFA spectra are similar in the appearance of the peaks, although there are some variations in term of peak intensity. It is noticed that no C═C characteristic peak is found at 1660–1630 cm^{-1}, indicating the completed polymerization of the monomer [37]. The small peaks appearing at 2852 cm^{-1}, 2920 cm^{-1} and 3030 cm^{-1} correspond to the aromatic and aliphatic C–H stretching bonds [38]. Several peaks are obtained between 1450 and 1610 cm^{-1} (e.g. 1604, 1496 and 1456 cm^{-1}) which match with the benzene ring C═C–C stretches and confirm the presence of benzene rings in the result PFA products. The two strong peaks at 700 and 758 cm^{-1} relate to the monosubstituted benzene ring and hence confirm the presence of styrene units in the result products [39]. The absorption at 2852 and 2920 cm^{-1} shows aliphatic (saturated) C–H groups. A sharp peak is obtained at 1750 cm^{-1} which corresponds to the presence of carbonyl C═O in ester group, and the shoulder at 1716 cm^{-1} corresponds to the carbonyl in carboxylic acid group. A wide peak around 3400–3500 cm^{-1} relates to the O–H stretching vibration and the other peak at 909 cm^{-1} corresponds to the non-planar angular vibration of O–H group in carboxylic acids [37]. The FTIR result indicates the presence of acrylic acid structural unit in the products. Several complex absorption peaks between 1280 and 1120 cm^{-1} are attributed to the $-CF_2$ group. $CF-CF_3$ group absorbs strongly at 735 cm^{-1}, and the absorption at 1350 cm^{-1} may be assigned to $-CF_3$ group. Since the intense carbonyl peak at 1750 cm^{-1} belongs to the ester group, heptafluorobutyl acrylate structural unit is verified in the result products [40].

Table 2
Atomic ratios of major elements of PFA films produced from different HBA/styrene molar ratios.

HBA/styrene ratio	C 1 s %	F 1 s %	O 1 s %
0.75	54.4	26.0	19.5
1	54.0	28.9	17.0
2	48.5	34.0	18.6

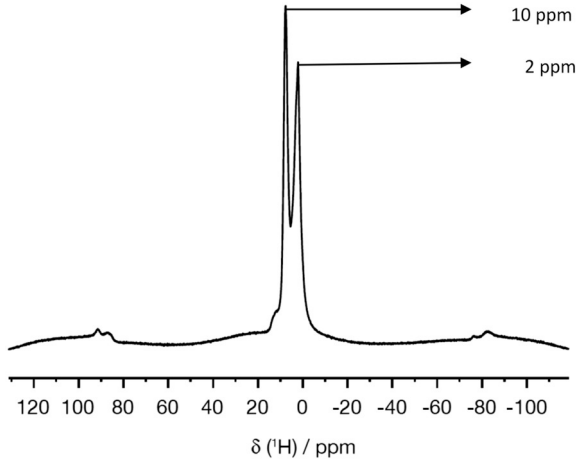

Fig. 2. ^1H NMR analysis data for PFA emulsion containing 16.6 wt% of fluorine.

The amount of monomer units in the PFA emulsion is determined by calculating the relative absorbance of absorption bands as A/A_0 using the baseline method, where A_0 is the internal standard. In this study, the benzene ring C═C–C stretching vibration peak of styrene unit at 1604 cm^{-1} is taken as the internal standard [37]. The calculation results show that the amount of acrylic acid unit in PFA 10.2 is slightly more than that in PFA 10.1, and the amount of the heptafluorobutyl acrylate unit in PFA 10.2 is significantly higher than that in PFA 10.1.

By comparing the above FTIR data, it is observed that identical C–F bonds contained in PFA10.1 and PFA10.2 spectra irrespective of the fluorine amount in the polymers. Therefore, the basic reaction mechanism and products remain unaltered, with different amount of heptafluorobutyl acrylate involved in the polymerization.

Table 2 shows atomic percentages of carbon (C), fluorine (F), and oxygen (O) in the PFA films synthesized using different molar ratios of heptafluorobutyl acrylate. The molar ratio of styrene and acrylic acid was kept constant at 1:1. With the increase of the HBA addition, fluorine atomic ratio in the PFA films gradually increases. The atomic ratios of carbon and oxygen vary as well, indicating the formation of *co*-polymer structures containing a various number of monomer units. When the HBA/styrene ratio is 0.75, the atomic ratio of carbon/fluorine/oxygen of the film is 2.8:1.3:1. When the HBA ratio raises to 2, the C:F:O atomic ratio of the film stands at 2.6:1.8:1. The overall

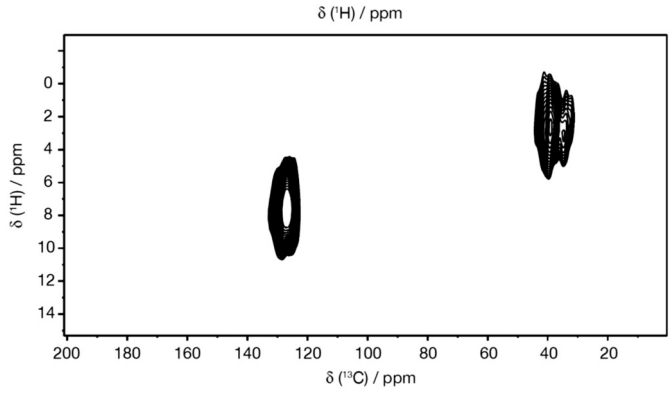

Fig. 3. ^{13}C NMR analysis for PFA emulsion containing 16.6 wt% of fluorine.

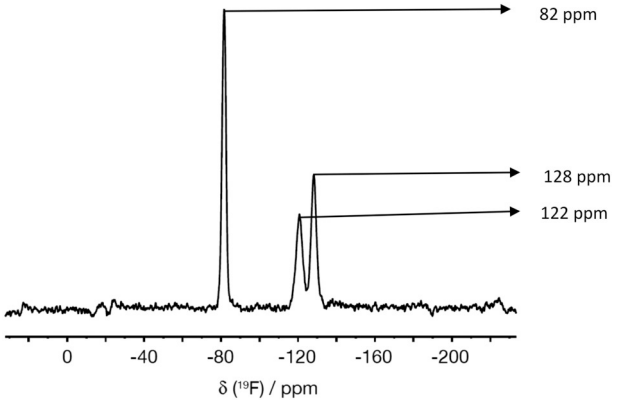

Fig. 4. ^{19}F NMR analysis data for PFA emulsion containing 16.6 wt% of fluorine.

fluorine atomic percentage significantly increases in the PFA polymer.

3.2. NMR analysis

NMR analysis for ^{1}H, ^{13}C, and ^{19}F NMR was conducted to determine the groups present in the synthesized PFA emulsion.^{1}H spectrum in Fig. 2 shows two peaks which means that there are two types of hydrogens in the compound and both of them are in a totally different environment. Two peaks are obtained at 2 ppm and 10 ppm, respectively, and both of them are sharp with high intensity. The starting materials were styrene, acrylic acid, and heptafluorobutyl acrylate and hence two types of hydrogen were involved: aromatic hydrogen of the benzene ring and aliphatic hydrogen atoms from the other two monomers. The existence of two peaks indicates that the aromatic ring of styrene remains in the final product and no ring opening reaction has taken place. The peak with a larger chemical shift from zero (10 ppm) is for the aromatic hydrogen coming from the styrene. The chemical shift for aromatic hydrogens is usually in the range of 5–7 ppm [41]. The higher chemical shift here may be attributed by the substation of the aromatic ring by a large aliphatic chain. Another peak with relatively lower chemical shift value (2 ppm) is for the aliphatic hydrogens.

To support the ^{1}H NMR analysis, further ^{13}C NMR was also carried out. Fig. 3 depicts the ^{13}C NMR peaks for the same PFA emulsion. It also shows two peaks, confirming the presence of two types of C atoms in the compound. Similarly, the peak with a large chemical shift in the region of 120–140 ppm [42] corresponds to the carbon atoms in an aromatic ring of styrene. The greater chemical shift for aromatic carbon atom is due to the high electron density on the aromatic ring. The chemical shift region of 20–40 ppm corresponds to the aliphatic carbon atoms. Overall, the ^{13}C NMR also supports the result obtained for ^{1}H NMR in Fig. 2.

Finally, ^{19}F NMR in Fig. 4 shows three peaks at 82 ppm, 122 ppm, and 128 ppm. These peaks correspond to $-CF_3$, $-CF_2$ and $-CF_2$ of heptafluorobutyl acrylate, respectively, as the group of $CF_3-CF_2-CF_2-$ [43]. The two $-CF_2$ groups will have different peak positions due to their different surroundings. The peak at 128 ppm corresponds to the $-CF_2$ group that is directly connected to the CF_3 group and another $-CF_2$ group. The higher chemical shift is due to the increased interaction with a greater number of fluorine atoms of surrounding CF_2 and CF_3 group. The peak at 122 ppm corresponds to outer $-CF_2$ groups of the $-CF_2-CF_2-CF_3$ chain and ultimately the peak at 82 ppm corresponds to the fluorine atoms in $-CF_3$ group. These peaks also integrate to 3:2:2 respectively for CF_3:CF_2:CF_2, indicating that no other fluorine groups are present.

From the starting monomers, the possible chain structures formed in the polymerization are sketched in Fig. 5. According to the FTIR and NMR analysis results, the most convincing structure is a *co*-polymer structure including styrene, acrylic acid, and heptafluorobutyl acrylate. The number of monomer units in a repeating unit is fixed as expected from a radical polymerization reaction. Therefore, the schematic structure of the polymer before crosslinking is proposed in Fig. 6. This is the schematic repeating unit of the polymer. The fluorine groups are towards the surface, which may provide the desired hydrophobicity.

3.3. Reaction mechanism

The reactions occur via radical polymerization at 80 °C in a reflux condenser and the final crosslinking occurs at a temperature of 80 °C in vacuum oven. A stepwise reaction mechanism is proposed via the following reactions:

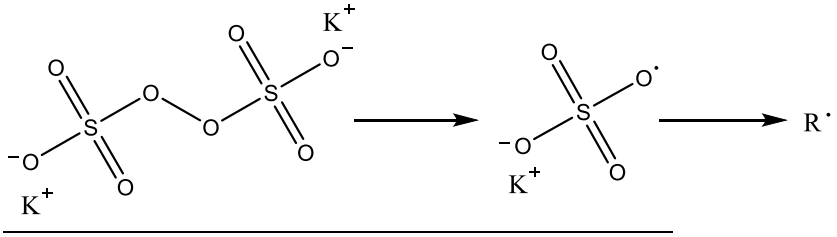

(1)

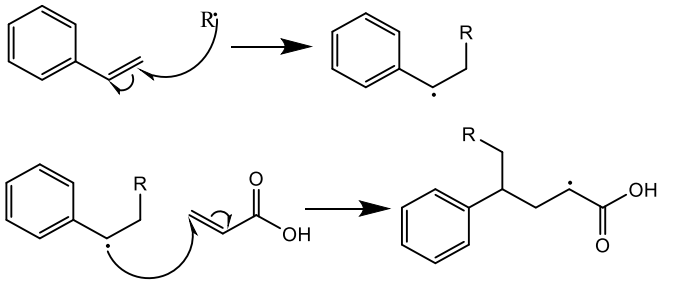

(2)

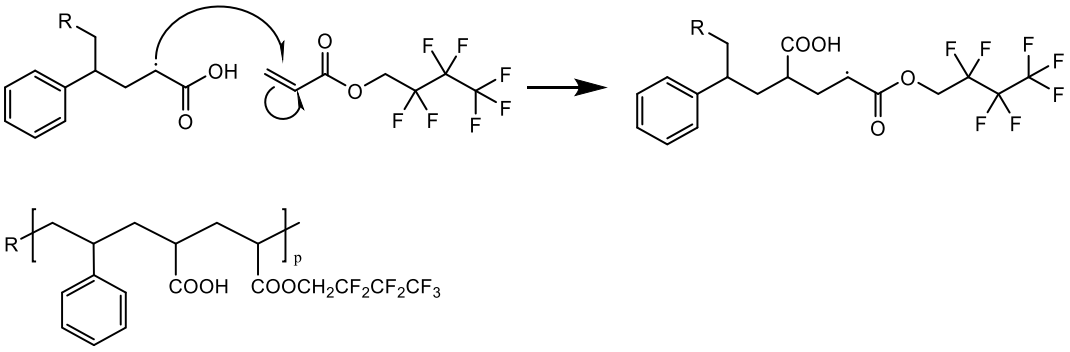

(3)

Reaction (2) and (3) can be combined and written as follows:

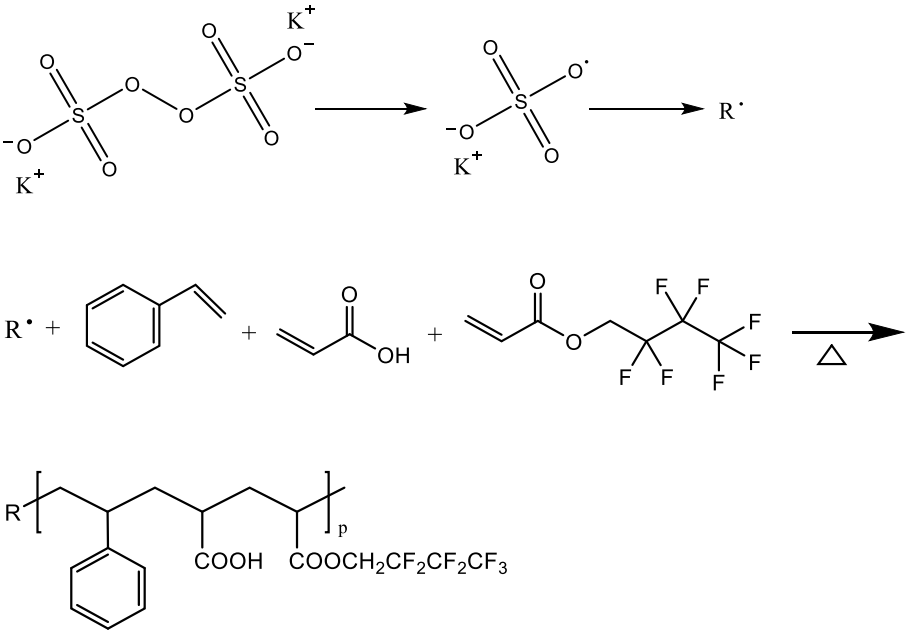

(4)

Potassium persulfate (KPS) in the reactions acts as an initiator. It dissociates along the −O−O− bond and forms the initiator as shown in reaction (1). The initiator concentration is important as it directly affects the reaction rate of the radical initiated polymerization [44]. The decomposition rate of KPS also follows the first order reaction kinetics and the reaction rate increases at elevated temperature [45]. Also, the presence of free monomolecular dispersed sodium dodecylsulfate (SDS) promotes the decomposition of KPS whereas some SDS molecules form micelle and get adsorbed on the polystyrene particles and hence do not contribute to the decomposition of KPS [46]. To simplify the reaction mechanism, only a single unit of the monomer is being used for polymerization. The free radical formed by the decomposition of KPS attacks the $-C_2H_3$ group of styrene and forms another radical as shown in reaction (2). It attacks the outer carbon atom of $-C_2H_3$ group due to less steric hindrance. The activated styrene then reacts with the outer carbon atom of C═C of acrylic acid and forms an oligomer of radical of styrene and acrylic acid depicted in reaction (3). The reaction continues as the newly produced radical reacts with the C═C of heptafluorobutyl acrylate. NMR and FTIR results confirm all monomer units are clearly involved in the *co*-polymerization. But for a radical polymerization reaction, random co-polymers are normally formed with varying number of monomer units.

3.4. Thermal analysis

Fig. 7 shows the variation of mass change (wt%) and heat flow of the PFA emulsion (PFA 10.1) as a function of temperature. Initially, both the heat flow and the mass decrease rapidly as the temperature increases to 73 °C, attributing to the evaporation of the solvent (e.g. water). After 73 °C, the heat flow of the sample gradually increases, indicating the start of curing of the sample, while the mass continues to decrease and becomes stable after 100 °C. The heat flow of the sample increases until 120 °C, and then keeps at 0, indicating that no more reaction occurs after 120 °C. It is suggested that the curing temperature of the polymer ranges from 73 to 120 °C. The tested polymer cannot be re-melted and maintains a stable state at a high temperature, reflecting a thermosetting nature.

3.5. Hydrophobicity of the PFA film

The PFA emulsions containing different fluorine contents were spin coated on the aluminium substrates. The wettability of the film surface was quantified by the water contact angle.

Fig. 8 shows the surface wettability of PFA10.1 film versus the curing temperature. All the curing duration was fixed for 2 h. It is observed that the highest water contact angle is obtained at 80 °C. With the increase in curing temperature to 120 °C, the water contact angle decreases to some extent; and the film curing at 180 °C led to the

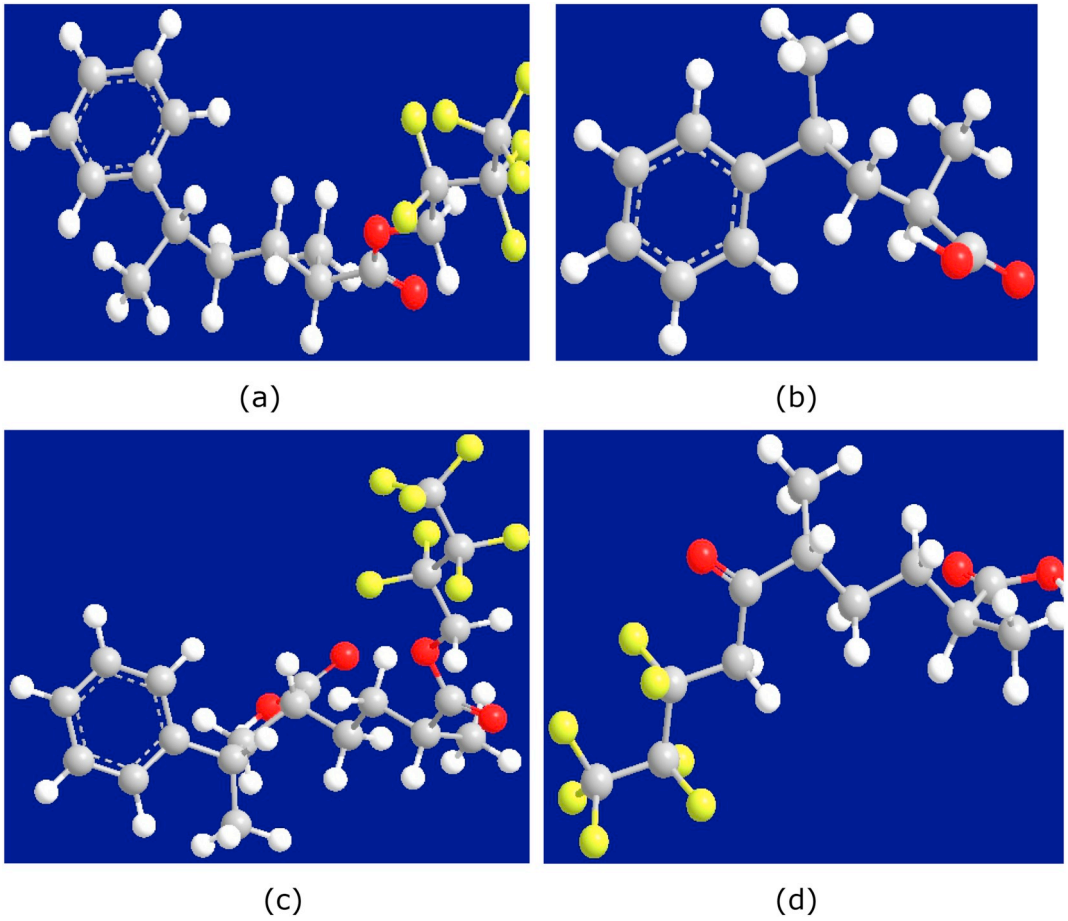

Fig. 5. Possible chain structures formed in the polymerization: (a) *co*-polymer of Styrene and heptafluorobutyl acrylate, (b) *co*-polymer of styrene and acrylic acid, (c) co-polymer of styrene acrylic acid and heptafluorobutyl acrylate and (d) co-polymer of acrylic acid and heptafluorobutyl acrylate. The red balls refer to oxygen atoms, the yellow respresent fluorine, the white correspond to the hydrogen atoms, and the grey balls are carbon atoms.

contact angle around 112–114°. With the increase of temperature, the crosslinking rate increases and some of the surface fluorine groups may be masked by other less hydrophobic groups and hence caused a slight increase in wettability.

The surface wettability of the films changes drastically with the molar ratio of HBA as evidenced from Fig. 9. In all the cases, the molar ratio of styrene and acrylic acid was kept at 1:1, and only the ratio of HBA was altered. The highest water contact angle 121 °C was achieved when the molar ratio of HBA was 0.75. All the films were cured at 80 °C for 2 h. When the ratio of HBA was 0.5, the concentration of HBA seemed to be too low to offer a better hydrophobicity. However, when the molar ratio of HBA reached to 1 or 2, the water contact angle also dropped slightly, which may be attributed to the oversaturation of the surface. The atomic percentage of fluorine in the PFA film gradually increases from 26.0% to 34.0% when the ratio of HBA increased from 0.75 to 2. It is observed that once the HBA/styrene molar ratio reached 0.75, more HBA did not lead to the further increase of surface hydrophobicity, and slight reduction of WCA was observed at HBA/styrene molar ratio of 1 and 2. The surface roughness Ra of the PFA films was measured. It is found that initially the average surface roughness Ra rises from 0.216 μm to 0.236 μm when the HBA/styrene molar ratio increases from 0.5 to 0.75. With further increase in HBA ratio to 1 and 2, the average surface roughness Ra slightly decreases to 0.224 and 0.220 μm, respectively. As surface hydrophobicity depends on both surface roughness and surface energy, the decrease of WCA at higher HBA/styrene ratio is attributed to the small reduction of surface roughness.

3.6. Ice adhesion strength of the PFA film

The ice adhesion strength of the PFA films was evaluated by the centrifugal method. Fig. 10 shows the variation of ice adhesion strength of the glaze ice attached on the sample surface measured at −10 °C. Lower ice adhesion strength is a desirable requirement for de-icing operation. The average ice adhesion strength is dependent on equilibrium contact angle (θ_e) by the variable of $1 + cos\theta_e$ [42]. Thus, with increasing hydrophobicity, low ice adhesion strength can be obtained. The result indicated a clear decrease in ice adhesion strength from 146 KPa to 44 KPa when the aluminium substrate surface was covered with a PFA film. By comparing the surface roughness and fluorine content of both PFA films, it is suggested that the decrease of ice adhesion strength is mainly contributed from the increase of the fluorine content in the PFA film. The heptafluorobutyl group of the polymer provides lowered surface energy, offering reduced bonding strength with ice.

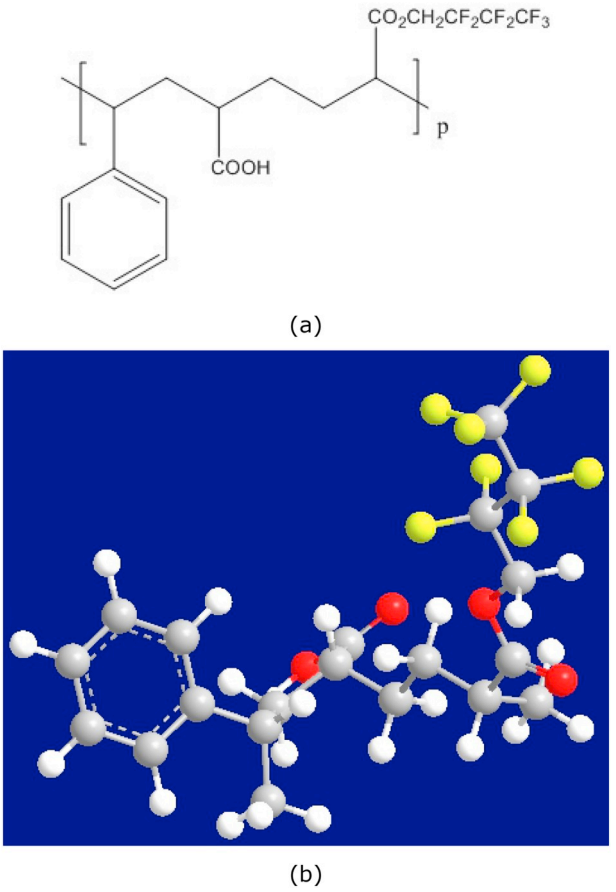

Fig. 6. (a) 2D and (b) 3D chain structures of the synthesized co-polymer prior to cross-linking. The red atoms refer to oxygen atoms, the yellow represent fluorine, the white correspond to the hydrogen atoms, and the grey balls are carbon atoms.

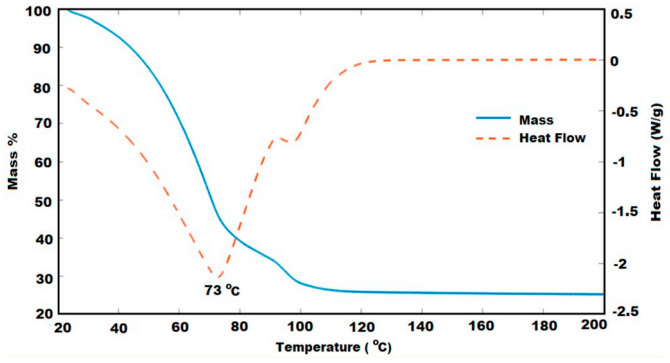

Fig. 7. Variation of mass change (wt%) and heat flow of PFA emulsion (PFA 10.1) with increasing temperature.

4. Conclusions

A two-step process of synthesizing styrene-based *co*-polymer emulsion has been developed, and hydrophobic polyfluoroacrylate films have been deposited by spin coating process. The co-polymer is synthesized via radical polymerization of styrene, acrylic acid, and heptafluorobutyl acrylate resulting in the formation of random co-polymer structure. The curing of the synthesized polymer could occur at a relatively low temperature (80 °C). The polymer film with relatively low surface roughness shows good hydrophobicity with a water contact angle up to 121°. The atomic ratios of carbon, fluorine, and oxygen in the PFA films vary with HBA/styrene molar ratio of the starting monomers. The fluorine content in the polymer increases with increasing concentration of HBA, which affects both surface hydrophobicity and icephobicity. Ice adhesion test shows that the PFA film has clearly reduced ice adhesion strength as compared to the uncoated reference. And the ice adhesion strength of the PFA films decreased with the increase of the fluorine content.

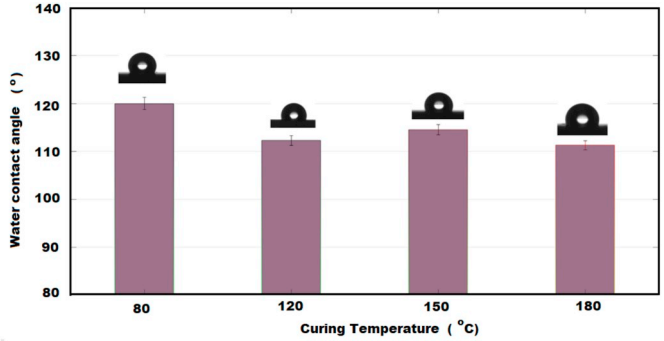

Fig. 8. Surface wettability versus curing temperature of PFA 10.1.

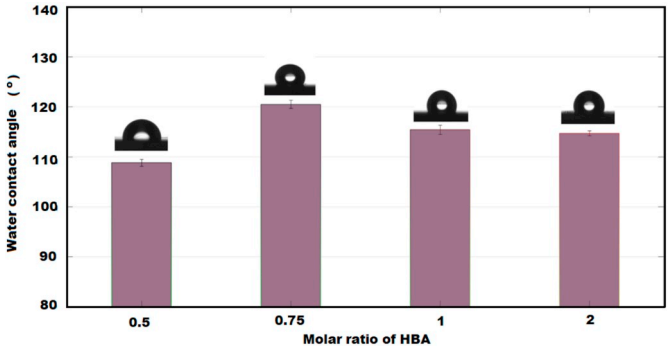

Fig. 9. Surface wettability of the film versus the molar ratio of heptafluorobutyl acrylate.

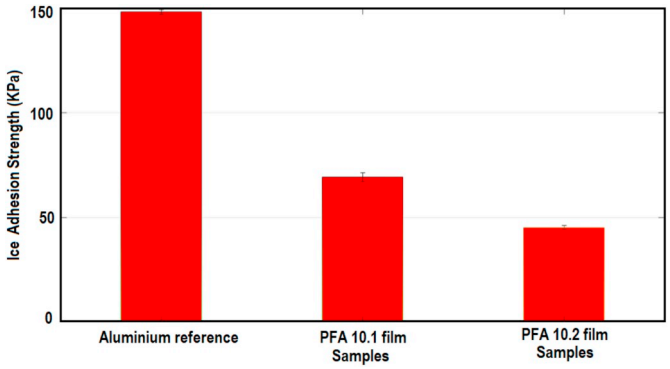

Fig. 10. Ice adhesion strength of the coating samples and aluminium reference at −10 °C.

Acknowledgements

This work was supported by Intercampus PhD Scholarship, University of Nottingham, UK. The authors would also like to thank Nanoscale and Microscale Research Centre (NMRC) at University of Nottingham for providing access to the instrumentation.

References

[1] L. Cao, A.K. Jones, V.K. Sikka, J. Wu, D. Gao, Anti-icing superhydrophobic coatings, Langmuir 25 (2009) 12444–12448.
[2] S.A. Kulinich, S. Farhadi, K. Nose, X.W. Du, Superhydrophobic surfaces: are they really ice-repellent? Langmuir 27 (2011) 25–29.
[3] M. Ma, R.M. Hill, Superhydrophobic surfaces, Curr. Opin. Colloid Interface Sci. 11 (2006) 193–202.
[4] C.-H. Xue, S.-T. Jia, J. Zhang, J.-Z. Ma, Large-area fabrication of superhydrophobic surfaces for practical applications: an overview, Sci. Technol. Adv. Mater. 11 (2010) 033002.
[5] M. Susoff, K. Siegmann, C. Pfaffenroth, M. Hirayama, Evaluation of icephobic coatings—screening of different coatings and influence of roughness, Appl. Surf. Sci. 282 (2013) 870–879.
[6] M.A. Samaha, H.V. Tafreshi, M. Gad-el-Hak, Superhydrophobic surfaces: from the lotus leaf to the submarine, C. R. Mécanique 340 (2012) 18–34.
[7] X. Zhang, F. Shi, J. Niu, Y. Jiang, Z. Wang, Superhydrophobic surfaces: from structural control to functional application, J. Mater. Chem. 18 (2008) 621–633.
[8] X.-M. Li, D. Reinhoudt, M. Crego-Calama, What do we need for a superhydrophobic surface? A review on the recent progress in the preparation of superhydrophobic surfaces, Chem. Soc. Rev. 36 (2007) 1350–1368.
[9] B. Qian, Z. Shen, Fabrication of superhydrophobic surfaces by dislocation-selective chemical etching on aluminum, copper, and zinc substrates, Langmuir 21 (2005) 9007–9009.
[10] K. Tsujii, T. Yamamoto, T. Onda, S. Shibuichi, Super Oil-Repellent Surfaces, Angew. Chem. Int. Ed. Eng. 36 (1997) 1011–1012.
[11] A.V. Rao, A.B. Gurav, S.S. Latthe, R.S. Vhatkar, H. Imai, C. Kappenstein, P.B. Wagh, S.C. Gupta, Water repellent porous silica films by sol–gel dip coating method, J. Colloid Interface Sci. 352 (2010) 30–35.
[12] B. Bhushan, Y.C. Jung, Micro-and nanoscale characterization of hydrophobic and hydrophilic leaf surfaces, Nanotechnology 17 (2006) 2758.
[13] L. Jiang, Y. Zhao, J. Zhai, A lotus-leaf-like superhydrophobic surface: a porous microsphere/nanofiber composite film prepared by electrohydrodynamics, Angew. Chem. 116 (2004) 4438–4441.
[14] T. Baldacchini, J.E. Carey, M. Zhou, E. Mazur, Superhydrophobic surfaces prepared by microstructuring of silicon using a femtosecond laser, Langmuir 22 (2006) 4917–4919.
[15] A. Dotan, H. Dodiuk, C. Laforte, S. Kenig, The relationship between water wetting and ice adhesion, J. Adhes. Sci. Technol. 23 (2009) 1907–1915.
[16] Q. Fu, X. Wu, D. Kumar, J.W.C. Ho, P.D. Kanhere, N. Srikanth, E. Liu, P. Wilson, Z. Chen, Development of sol–gel icephobic coatings: effect of surface roughness and surface energy, ACS Appl. Mater. Interfaces 6 (2014) 20685–20692.
[17] V.F. Petrenko, S. Peng, Reduction of ice adhesion to metal by using self-assembling monolayers (SAMs), Can. J. Phys. 81 (2003) 387–393.
[18] P.A. Levkin, F. Svec, J.M. Frechet, Porous polymer coatings: a versatile approach to superhydrophobic surfaces, Adv. Funct. Mater. 19 (2009) 1993–1998.
[19] K.S. Min, Y. Inseong, C.W. Kyung, S.H. Kyong, L.T. Geol, I.S. Choi, J.M. Karp, L. Haeshin, One-step modification of superhydrophobic surfaces by a mussel-inspired polymer coating, Angew. Chem. Int. Ed. 49 (2010) 9401–9404.
[20] H.Y. Erbil, A.L. Demirel, Y. Avcı, O. Mert, Transformation of a simple plastic into a superhydrophobic surface, Science 299 (2003) 1377–1380.
[21] D.K. Sarkar, M. Farzaneh, R.W. Paynter, Superhydrophobic properties of ultrathin rf-sputtered Teflon films coated etched aluminum surfaces, Mater. Lett. 62 (2008) 1226–1229.
[22] X. Su, H. Li, X. Lai, L. Zhang, T. Liang, Y. Feng, X. Zeng, Polydimethylsiloxane-based superhydrophobic surfaces on steel substrate: fabrication, reversibly extreme wettability and oil–water separation, ACS Appl. Mater. Interfaces 9 (2017) 3131–3141.
[23] N. Saleema, D.K. Sarkar, R.W. Paynter, X.G. Chen, Superhydrophobic aluminum alloy surfaces by a novel one-step process, ACS Appl. Mater. Interfaces 2 (2010) 2500–2502.
[24] S. Wang, L. Feng, L. Jiang, One-step solution-immersion process for the fabrication of stable bionic superhydrophobic surfaces, Adv. Mater. 18 (2006) 767–770.
[25] S. Ozbay, C. Yuceel, H.Y. Erbil, Improved icephobic properties on surfaces with a hydrophilic lubricating liquid, ACS Appl. Mater. Interfaces 7 (2015) 22067–22077.
[26] M. Gerard, C.R. Bowen, F.H. Osman, Processing and properties of PTFE-FEP-PTFE ferroelectret films, Ferroelectrics 422 (2011) 59–64.
[27] J. Jiang, L. Zhu, L. Zhu, B. Zhu, Y. Xu, Surface characteristics of a self-polymerized dopamine coating deposited on hydrophobic polymer films, Langmuir 27 (2011) 14180–14187.
[28] Z. Hua, W. Hongxia, N. Haitao, G. Adrian, W. Xungai, L. Tong, Fluoroalkyl silane modified silicone rubber/nanoparticle composite: a super durable, robust superhydrophobic fabric coating, Adv. Mater. 24 (2012) 2409–2412.
[29] R. Menini, Z. Ghalmi, M. Farzaneh, Highly resistant icephobic coatings on aluminum alloys, Cold Reg. Sci. Technol. 65 (2011) 65–69.
[30] S. Zhang, J. Huang, Y. Cheng, H. Yang, Z. Chen, Y. Lai, Bioinspired surfaces with superwettability for anti-icing and ice-phobic application: concept, mechanism, and design, Small 13 (2017) 1701867.
[31] S. Ozbay, H.Y. Erbil, Ice accretion by spraying supercooled droplets is not dependent on wettability and surface free energy of substrates, Colloids Surf. A Physicochem. Eng. Asp. 504 (2016) 210–218.
[32] M. Zou, S. Beckford, R. Wei, C. Ellis, G. Hatton, M.A. Miller, Effects of surface roughness and energy on ice adhesion strength, Appl. Surf. Sci. 257 (2011) 3786–3792.
[33] C. Wang, M.C. Gupta, Y.H. Yeong, K.J. Wynne, Factors affecting the adhesion of ice to polymer substrates, J. Appl. Polym. Sci. 135 (2018) 45734.
[34] A. Davis, Y.H. Yeong, A. Steele, I.S. Bayer, E. Loth, Superhydrophobic nanocomposite surface topography and ice adhesion, ACS Appl. Mater. Interfaces 6 (2014) 9272–9279.
[35] A.J. Meuler, J.D. Smith, K.K. Varanasi, J.M. Mabry, G.H. McKinley, R.E. Cohen, Relationships between water wettability and ice adhesion, ACS Appl. Mater. Interfaces 2 (2010) 3100–3110.
[36] Z.A. Janjua, B. Turnbull, K.-L. Choy, C. Pandis, J. Liu, X. Hou, K.-S. Choi, Performance and durability tests of smart icephobic coatings to reduce ice adhesion, Appl. Surf. Sci. 407 (2017) 555–564.
[37] G. Socrates, Infrared and Raman Characteristic Group Frequencies: Tables and Charts, John Wiley & Sons, 2004.
[38] E. Pretsch, P. Buehlmann, C. Affolter, E. Pretsch, P. Bhuhlmann, C. Affolter, Structure Determination of Organic Compounds, Springer, 2000.
[39] N. Solcà, O. Dopfer, Protonated benzene: IR spectrum and structure of C6H7, Angew. Chem. Int. Ed. 41 (2002) 3628–3631.
[40] D. Lin-Vien, N.B. Colthup, W.G. Fateley, J.G. Grasselli, The Handbook of Infrared and Raman Characteristic Frequencies of Organic Molecules, Elsevier, 1991.
[41] R.M. Silverstein, G.C. Bassler, Spectrometric identification of organic compounds, J. Chem. Educ. 39 (1962) 546.
[42] E. Pretsch, T. Clerc, J. Seibl, W. Simon, Tables of Spectral Data for Structure Determination of Organic Compounds, Springer Science & Business Media, 2013.
[43] A. Svensson, T. Fex, J. Kihlberg, Use of 19F NMR spectroscopy to evaluate reactions in solid phase organic synthesis, Tetrahedron Lett. 37 (1996) 7649–7652.
[44] H.-R. Lin, Solution polymerization of acrylamide using potassium persulfate as an initiator: kinetic studies, temperature and pH dependence, Eur. Polym. J. 37 (2001) 1507–1510.
[45] K. Kinoshita, Y. Takano, N. Ohkouchi, S. Deguchi, Free-radical polymerization of acrylic acid under extreme reaction conditions mimicking Deep-Sea hydrothermal vents, ACS Omega 2 (2017) 2765–2769.
[46] O. Masayoshi, M. Toshiyuki, The decomposition of potassium persulphate used as initiator in emulsion polymerization, Makromol. Chem. Macromol. Symp. 31 (1990) 143–156.